Thin Solid Films 520 (2012) 6215–6220

Contents lists available at SciVerse ScienceDirect

Thin Solid Films

journal homepage: www.elsevier.com/locate/tsf

Organic photovoltaic cells fabricated on a $SnO_x/Ag/SnO_x$ multilayer transparent conducting electrode

Jeong-Do Yang [a,b], Se-Hee Cho [a], Tae-Woo Hong [a], Dong Ick Son [a], Dong-Hee Park [a], Kyung-Hwa Yoo [b], Won-Kook Choi [a,*]

[a] Interface Control Research Center, Korea Institute of Science and Technology, Sungbuk-Gu, Hwarangno 14-gil 5, Seoul 136-791, Republic of Korea
[b] Department of Physics, Yonsei University, 134 Sinchon-Dong, Seodaemun-Gu, Seoul 120-749, Republic of Korea

ARTICLE INFO

Article history:
Received 18 September 2011
Received in revised form 9 May 2012
Accepted 18 May 2012
Available online 24 May 2012

Keywords:
Tin oxide
Silver
Multilayer transparent conducting electrode
Electrical resistivity
Optical transmittance
Organic photovoltaic cell
Power conversion efficiency

ABSTRACT

Transparent conducting multilayer structured electrode of a few nm Ag layer embedded in tin oxide thin film $SnO_x/Ag/SnO_x$ was fabricated on a glass by RF magnetron sputtering at room temperature. The multilayer of the SnO_x(40 nm)/Ag(11 nm)/SnO_x(40 nm) electrode shows the maximum optical transmittance of 87.3% at 550 nm and a quite low electrical resistivity of $6.5\times10^{-5}\,\Omega$ cm, and the corresponding figure of merit (T^{10}/R_S) is equivalent to $3.6\times10^{-2}\,\Omega^{-1}$. A normal organic photovoltaic (OPV) structure of poly(3,4-ethylenedioxythiophene): poly(styrene sulfonate)/polythiophene:phenyl-C60-butyric acid methyl ester/Al was fabricated on glass/SnO_x/Ag/SnO_x to examine the compatibility of OPV as a transparent conducting electrode. Measured characteristic values of open circuit voltage of 0.62 V, saturation current of 8.11 mA/cm^2 and fill factor of 0.54 are analogous to 0.63 V, 8.37 mA/cm^2 and 0.58 of OPV on commercial glass/indium tin oxide (ITO) respectively. A resultant power conversion efficiency of 2.7% is also very comparable with the 3.09% of the same OPV structure on the commercial ITO glass as a reference, and which reveals that $SnO_x/Ag/SnO_x$ can be appropriate to OPV solar cells as a sound transparent conducting electrode.

1. Introduction

Transparent conducting oxides (TCOs) such as the III-element (e.g., B, Al, Ga, In) doped zinc oxide are considered to be the most promising substitutes for costly indium–tin-oxide (ITO) in various types of optoelectronic devices [1–3] due to advantages, such as their high resistance to hydrogen plasma, non-toxicity, and cost-effectiveness. Their resistivity is nonetheless higher ($\rho = 2.5\text{–}4\times10^{-4}\,\Omega$ cm) than that ($\sim1\times10^{-4}\,\Omega$ cm) of ITO for optoelectronic devices such as panel displays and solar cells, making them less feasible for energy conversion applications [4]. As part of the considerable effort to develop alternative TCO materials, multilayer dielectric/metal/dielectric (DMD) materials have been suggested as candidates to overcome the limits of both the electrical resistivity and optical transmittance of single-layer TCOs. This is possible because the DMD structure can increase both the transparency in the visible wavelength range due to the anti-reflection properties of the successive layer coating of materials with a high (n_1)/low(n_2)/high(n_1) refractive index and the conductivity through carrier injection due to the difference in the work function at the interface between the metal and the transparent semiconducting oxide [5,6]. Sutthana et al. reported that AZO/Ag/AZO multilayer films deposited on a glass substrate exhibited a low figure of merit (T^{10}/R_S) of $6.9\times10^{-4}\,\Omega^{-1}$ and a power conversion efficiency of 0.61% when applied to a dye-sensitized solar cell [7]. To date, there have been few reports about organic photovoltaic (OPV) devices with normal structures which use acidic poly(3,4-ethylenedioxythiophene) (PEDOT):poly(styrene sulfonate) (PSS) as a hole transport layer on a DMD material (where the ZnO-related dielectric material used was a dielectric). Recently, Choi et al. fabricated an OPV device with an inverted cell structure using PEDOT:PSS on $ZnSnO_3/Ag/ZnSnO_3$; the efficiency of the organic solar cells was determined to be 2.55% on the multilayer structure with an improved figure of merit that is approximately $4.59\times10^{-2}\,\Omega^{-1}$. PEDOT:PSS (pH 1.5–2.5) was inversely coated onto an active layer as a hole transport layer considering that $ZnSnO_3$ is vulnerable to an acid solvent [8]. Due to the chemical instability of this formulation, an acid-resistant conducting electrode instead of ZnO will be necessary for the fabrication of an OPV device with a normal structure.

To date, there have been few reports about an OPV device with a normal structure using acidic PEDOT:PSS as a hole transport layer on a multilayer TCO. Given that SnO_2 is well known as a dielectric material with an excellent chemical stability [9], $SnO_x/Ag/SnO_x$ multilayers as a transparent conducting electrode were prepared by RF magnetron sputtering on a glass substrate. OPV devices with a normal structure were fabricated on $SnO_x/Ag/SnO_x$ multilayer electrodes in which the PEDOT:PSS layer was used as a hole transport layer. These devices were then characterized in terms of the open circuit voltage (V_{OC}), saturation current density (J_{SC}), fill factor (FF) and

* Corresponding author. Tel.: +82 2 958 5562; fax: +82 2 958 6720.
E-mail address: wkchoi@kist.re.kr (W-K. Choi).

0040-6090/$ – see front matter © 2012 Elsevier B.V. All rights reserved.
doi:10.1016/j.tsf.2012.05.029

power conversion efficiency (PCE). Also, the external quantum efficiency (EQE) of OPV was measured. They were compared to OPV devices with an ITO electrode as a reference.

2. Experimental details

A SnO_x/Ag/SnO_x multilayer was sputtered onto a pre-patterned glass substrate (Corning, Eagle XG 0.7 mm, Alkaline Earth Boro-Aluminosilicate) for the fabrication of the OPV device. The bottom SnO_x layer was sputtered at an RF power of 100 W and an Ar plasma gas pressure of 0.53 Pa. An Ag (RND Korea, Ag, 99.99%) intermediate metal layer was successively deposited by RF magnetron sputtering at 50 W under an Ar plasma gas pressure of 0.53 Pa. The surface microstructure and morphology of Ag films deposited on a SnO_x/glass substrate with the variations of Ag thickness were examined by using scanning electron microscopy (Jeol, JSM-6500F) operated at the acceleration voltage of 15 kV. Finally, the top SnO_x layer was sputtered via the same method used to sputter the SnO_x bottom layer using a SnO_2 ceramic target (LTS Research Laboratories, SnO_2, 99.99%). The distance between the substrate and the target was fixed at 70 mm during the sputtering process. This multilayer was developed so that the electrodes for the OPV device were patterned and then exposed to N_2 plasma under atmospheric pressure for 2 min to make the surface of the upper SnO_x layer hydrophilic. In a glove box, a PEDOT:PSS layer was spin-coated at 4000 rpm for 35 s onto the samples and annealed at 110 °C for 5 min on a hot plate. A bulk-hetero junction layer was also spin-coated at 3000 rpm for 15 s from a solution of polythiophene (P3HT):phenyl-C60-butyric acid methyl ester (PCBM) (17 mg/mL, 1:0.8 by volume) in dichlorobenzene [10]. After the evaporation of the solvent, the sample was loaded into a vacuum chamber and an Al thin film at 150 nm was deposited as a cathode electrode. An annealing process was then carried out at 150 °C for 10 min on a hot plate. Schematic diagrams depicting the overall device structure of the OPV are illustrated in Fig. 1. The electrical resistivity, carrier concentration, and mobility of the multilayer were measured by the Hall measurement system (Ecopia HMS 3000). The optical transmittance (T) was obtained by a UV–vis spectrophotometer (Perkin Elmer UV/Vis spectrometer Lambda 18) in a wavelength range of 200–900 nm. The active area of the fabricated devices was 0.09 cm^2. Photovoltaic measurements were done under illumination from a Xe 150 W solar simulator (Yamashita Denso YSS-50A) with AM 1.5 G filters. And OPVs with a cell area (0.2 cm^2) wider than the laser beam were also fabricated for the measurements of EQE. We measured EQE in the wavelength of 300 nm–800 nm using the QEX10 Quantum Efficiency Measurement System (PV Measurements, Inc.). For comparison, an identical OPV device was fabricated on a glass/ITO substrate ($R_s = 7\ \Omega$/sq, T = 89.4% at 550 nm) as a reference.

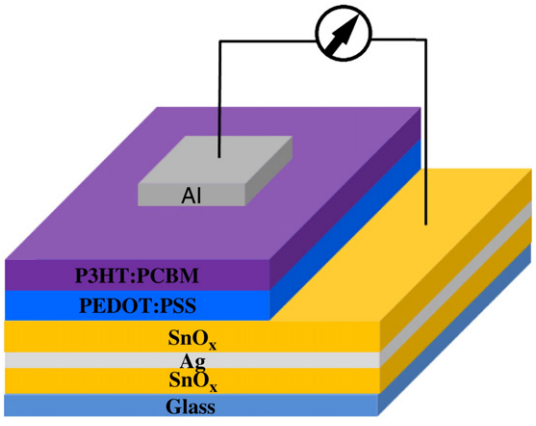

Fig. 1. Overall structure of the multilayer based OPV.

3. Results and discussion

3.1. Electrical and optical properties of the multilayer

In the SnO_x/Ag/SnO_x multilayer, Ag was selected as the metal layer due to its low electrical resistivity ($1\times10^{-6}\ \Omega$ cm) and its lower absorption in the visible wavelength compared to Cu and Au [11]. To determine the optimum thickness of the Ag layer, a thin Ag layer was deposited onto bare glass as well as the glass/SnO_x substrate for comparison. Fig. 2(a) shows the changes in the electrical resistivity of the Ag layer as the thickness varies. The change in the resistivity on both substrates is similar regardless of the thickness from 7 to 12 nm despite the fact that the resistivity of the Ag layer on the glass substrate is slightly lower than that on the glass/SnO_x substrate. The resistivity of the Ag layer on both substrates decreases considerably when the thickness ranges from 7 to 9 nm, after which it diminishes slightly even when the thickness momentarily peaks at 10 nm. At a thickness greater than 11 nm for glass/SnO_x/Ag, resistivity becomes as low as $6–7.5\times10^{-6}\ \Omega$ cm. Thus, the optimum thickness was at 11 nm so as not to decrease the transmittance further.

Fig. 2(b) illustrates the surface microstructure of the Ag layer on the glass/SnO_x substrate at different thicknesses using a scanning electron microscope. It is noteworthy that the surface morphology of the glass/SnO_x/Ag clearly becomes smooth when the thickness exceeds 9 nm. This result indicates that deposited Ag atoms cease to form Ag clusters, instead they take part in the formation of a continuous film at this critical thickness of 9–10 nm. This establishes that the resistivity of the Ag layer saturates to a certain value without a large variation, in the thickness above 10 nm. In addition, the optimized thickness of each SnO_x layer to minimize reflection was experimentally determined given the thickness showing a maximum transmittance of 11 nm of Ag by measuring the transmittance of fabricated SnO_x/Ag/SnO_x multilayers while varying the SnO_x thickness from 15 nm to 46 nm. It was found that multilayers with a SnO_x layer thicker than 36 nm show transmittance values that exceed 80% at 550 nm. As shown in Fig. 3(a), the optimized thickness of SnO_x for the highest transmittance (at 550 nm) of the multilayer with a fixed Ag thickness of 11 nm is 40 nm. For comparison, the transmittance of ITO and SnO_x(40 nm)/Ag(11 nm)/SnO_x(40 nm) is plotted in Fig. 3(b). The average transmittance of the multilayer in the wavelength range of 400–600 nm corresponding to the necessary energy level for an electron–hole pair to be generated in the active layer of P3HT:PCBM is 82.2% while the average transmittance of ITO in the same range is 87% [12,13]. $T_{400–600\ nm}$ is closely related to EQE, creating a difference in the photon flux that reaches the photon absorbing layer.

Fig. 4(a) shows a transmission electron microscope (TEM) image of a multilayer consisting of SnO_x(40 nm)/Ag(11 nm)/SnO_x(40 nm). Because the upper or bottom interfaces between SnO_x and Ag are both clearly distinguishable, it can be identified that the multilayer consists of a well-established sandwich structure at room temperature. Fig. 4(b) depicts the variation of the resistivity of the multilayer at various thicknesses of SnO_x. The resistivity of SnO_x(40 nm)/Ag(11 nm)/SnO_x(40 nm) was determined to be $6.5\times10^{-5}\ \Omega$ cm, which is quite low compared to the value of $1\times10^{-4}\ \Omega$ cm of ITO, which was used as a reference. Inserting the sheet resistance of each SnO_x and Ag layer (48.2 kΩ/square and 4.3 Ω/sq, respectively) into Eq. (1), the total sheet resistance of the multilayer is calculated as 4.3 Ω/square while the sheet resistance, measured by a four-point probe, is 7.1 Ω/square.

$$R_{total} = \left(\frac{2}{R_{SnO_x}} + \frac{1}{R_{Ag}}\right)^{-1} \quad (1)$$

Such a difference may result from a newly formed conducting path due to the Ag layer on the surface of the SnO_x layer or from some

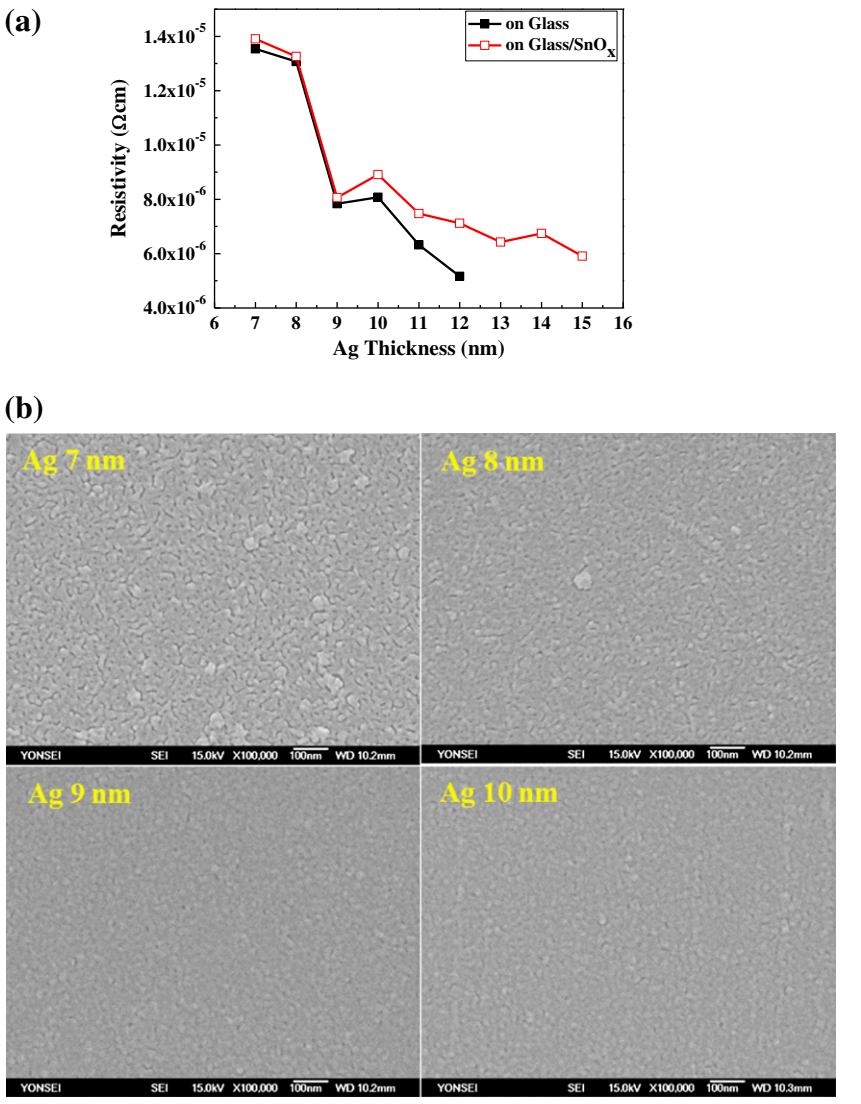

Fig. 2. (a) Electrical resistivity of Ag as thickness increases on both glass and glass/SnO_x. (b) SEM image of Ag films deposited on glass/SnO_x as Ag thickness was varied.

amount of theoretical error caused by limitations of a parallel circuit model. In the DMD multilayer structure, the electrical conduction is explained in terms of the carrier injection, which is mainly influenced by the difference in the work function at the interface between the metal and the transparent semiconducting oxide, as shown in Fig. 5. As shown in Fig. 5(a), the work function values of Ag and SnO_x are 4.26 eV and 4.74 eV, respectively. When these layers are brought into contact, the Fermi levels align at equilibrium due to the transfer of electrons from Ag to SnO_x. An accumulation type of contact between the Ag and the SnO_x is achieved due to band bending at the contact. In this case, because there is no barrier preventing an electron flow between the Ag and SnO_x, electrons are easily injected from the Ag layer into the SnO_x layer, as shown in Fig. 5(b) [14,15]. Based on the Schottky theory, we expect high carrier concentrations

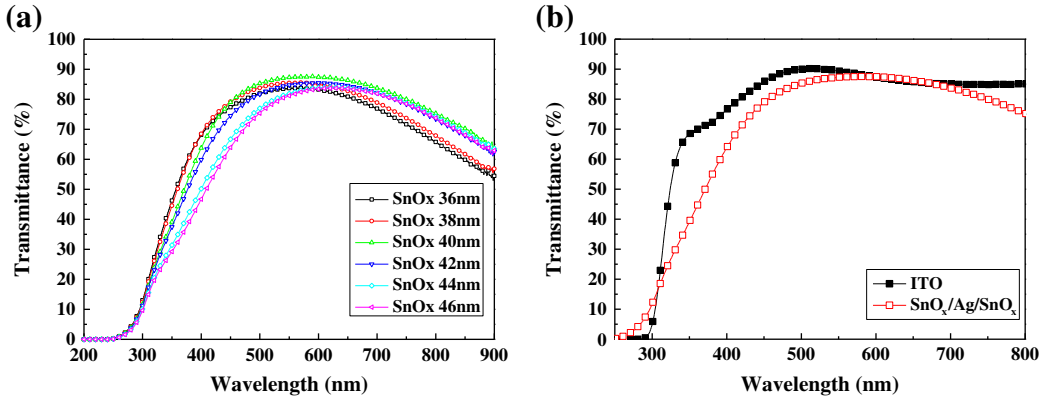

Fig. 3. (a) Transmittance of the multilayer as thickness of SnO_x increases. (b) Transmittance of a commercial ITO and the SnO_x/Ag/SnO_x multilayer.

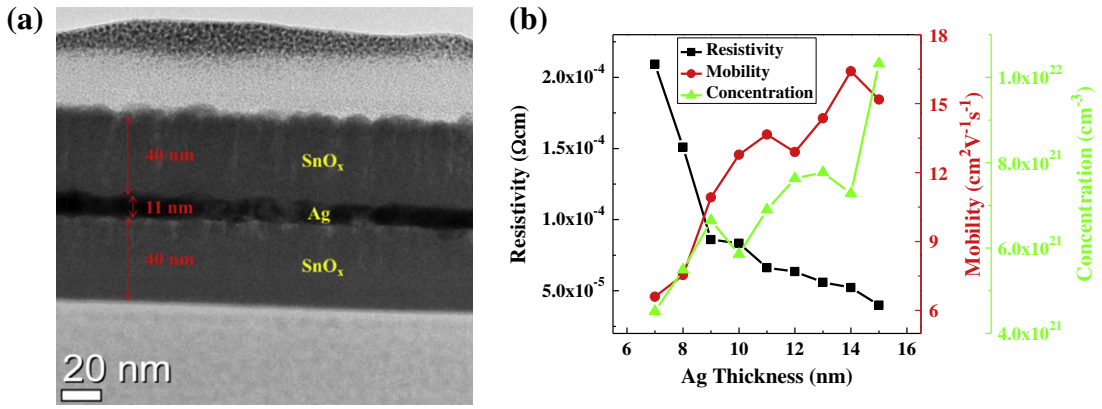

Fig. 4. (a) Cross sectional TEM image of the SnO_x/Ag/SnO_x multilayer structure. (b) Electrical properties of the multilayer as thickness of the Ag layer increases.

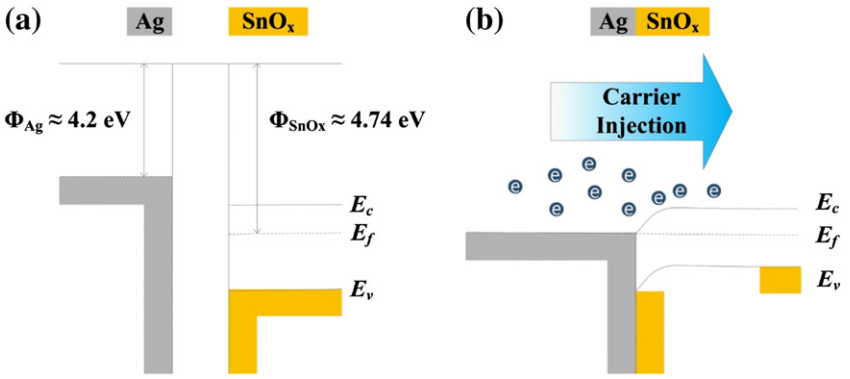

Fig. 5. Schematic diagrams of the energy band structures (a) before the contact between metal and n-type semiconductor. (b) Carrier injection after an accumulation type of Ohmic contact.

in the multilayer. The decrease in the resistivity with an increase in the Ag thickness can be attributed to the increased carrier concentration and mobility, as shown in Fig. 4(b). The electron mobility in single SnO_x films is 3.1 cm^2/V s. It rapidly increases as the Ag layer thickness increases from 6.6 cm^2/Vs at 7 nm to 16.4 cm^2/V s at 14 nm.

The figure of merit (F_{TC}) of a transparent conducting electrode is typically calculated using formula (2), as defined by Haacke [16]:

$$F_{TC} = \frac{T^{10}}{R_s}. \quad (2)$$

Here, R_s and T are the sheet resistance and the optical transmittance, respectively, at a wavelength of 550 nm. When the transmittance of 87.3% at 550 nm and the sheet resistance of 7.1 Ω/square are used in Eq. (2), a F_{TC} of $3.6\times10^{-2}\Omega^{-1}$ for the multilayer SnO_x(40 nm)/Ag(11 nm)/SnO_x(40 nm) is obtained; this is higher than the value of $1.2\times10^{-2}\Omega^{-1}$ of the reference ITO electrode.

3.2. OPV characterization

We tested the chemical compatibility of the SnO_x/Ag/SnO_x multilayer with an organic photovoltaic material. As mentioned earlier, ZnO-based TCO is vulnerable to an acid solution. Therefore, this bottleneck for a ZnO electrode when applied to a normal OPV device should be overcome. As shown in the optical microscope image in Fig. 6, when an AZO/Ag/AZO multilayer is exposed to a PEDOT:PSS

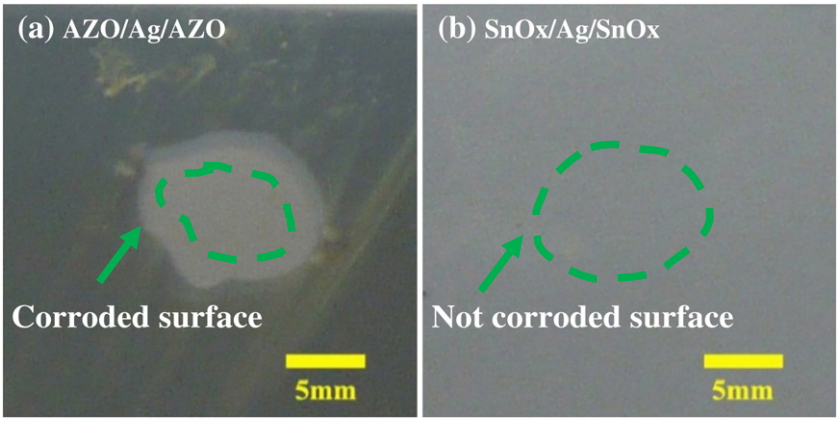

Fig. 6. Photograph images of (a) AZO/Ag/AZO and (b) SnO_x/Ag/SnO_x after exposure to PEDOT:PSS (acidity pH = 2–3) solution.

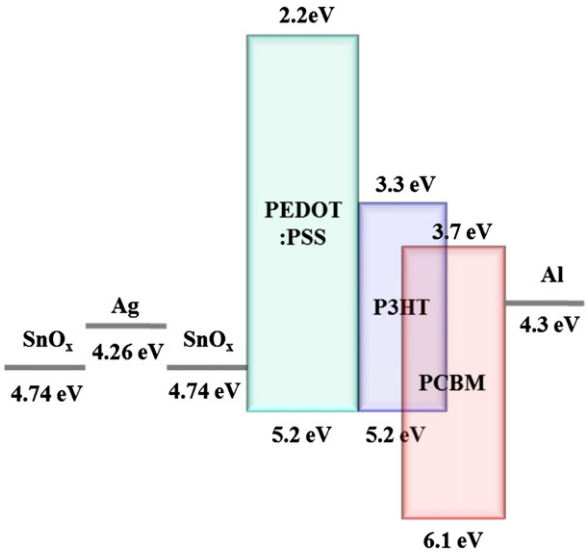

Fig. 7. Energy level diagram of OPVs with the normal structure.

(acidity pH = 2–3) solution, the upper and bottom AZO layers are completely peeled off along with the intermediate thin Ag layer. On the other hand, no noticeable change or damage to the SnO_x/Ag/SnO_x surface is observed after dropping PEDOT:PSS onto the surface. Thus, the SnO_x layer is believed to be chemically inert and quite compatible as a transparent electrode for an OPV device.

The energy level diagram for normal OPVs consisting of PEDOT:PSS/P3HT:PCBM is shown in Fig. 7. Fig. 8 shows the current density–voltage (J_{SC}–V_{OC}) characteristics under simulated illumination of AM 1.5 G (100 mW/cm^2) for OPVs (black squares for ITO, red squares for SnO_x/Ag/SnO_x). The performance of the OPV device fabricated on the multilayer electrode is summarized in Table 1. The normal OPV device fabricated on the multilayer electrode shows a V_{OC} of 0.62 V, a J_{SC} of 8.11 mA/cm^2, a (FF) of 0.54 and a PCE of 2.70%. These values are highly comparable to those of an identical OPV device on a conventional ITO structure, with a V_{OC} of 0.63 V, a J_{SC} value of 8.37 mA/cm^2, a FF of 0.58 and a PCE rating of 3.09%. The difference in the cell performance can be explained in terms of the J_{SC} and V_{OC} values, as well as the FF. The low J_{SC} value of the multilayer-based OPV device results from the low transmittance of its electrode as shown in Fig. 3(a), which leads to less photocurrent due to the low flux of the transmitted photon. The photocurrent generated by a solar cell under illumination under a short circuit condition is

Table 1
Characteristic measured values of the OPV fabricated on the SnO_x/Ag/SnO_x multilayer and commercial ITO as a reference.

Electrode	V_{OC} (V)	J_{SC} (mA/cm^2)	FF	PCE (%)
SnO_x/Ag/SnO_x	0.62	8.11	0.54	2.70
ITO	0.63	8.37	0.58	3.09

dependent on the incident light. To relate the photocurrent density (Eq. (3)), J_{SC}, to the incident spectrum, we need the cell's quantum efficiency (QE). QE is the probability that an incident photon of energy E will deliver one electron to an external circuit.

$$J_{SC} = q\int b_s(E)QE(E)dE \quad (3)$$

In this equation, $b_s(E)$ is the incident spectral photon flux density, the number of photons of energy in the range of E to E + dE which are incident on the unit area in unit time and q is the electronic charge. QE depends on the absorption coefficient of the solar cell material, the efficiency of charge separation and the efficiency of charge collection in the device but does not depend on the incident spectrum. Particularly, in the effective absorption range (400 nm–600 nm) of the active layer, the average transmittance of the multilayer is lower than that of commercial ITO, as shown in Fig. 3(b) and (c). Higher transmittance can deliver more photons and generate more photocurrent in the active layer, which results in a higher EQE in an OPV device on ITO [17–19]. This fact was to some extent supported by the EQE result. As shown in Fig. 9, the EQE of OPV fabricated on ITO was higher than that of the OPV on the SnO_x/Ag/SnO_x multilayer and which result would be mainly attributed to the difference of transmittance between them. Difference in sheet resistance will be another possible constraint to make a difference in device performance like EQE. Sheet resistances of the SnOx/Ag/SnOx and ITO electrodes were 7.1 Ω/square and 7 Ω/square respectively. But their series resistances in the fabricated OPV were $1.7\times10^2\,\Omega$ and $1.44\times10^2\,\Omega$ resulting from the difference in contact resistance between PEDOT:PSS and the transparent electrode. It is certainly admitted that a higher series resistance in practice may cause the lower J_{SC}, hence the efficiency becomes lower. Although the PCE of the multilayer is lower than that of the OPV device fabricated on the ITO electrode, the PCE of the OPV device fabricated on SnO_x/Ag/SnO_x is higher than any other previously reported OPV device with another type of multilayer [7,20]. This arises due to the increase in the transmittance, i.e., the photon flux, in the 400–600 nm wavelength and decrease in the sheet resistance. Therefore, the PCE of the OPV device can be improved by increasing EQE in the effective wavelength region of 400–

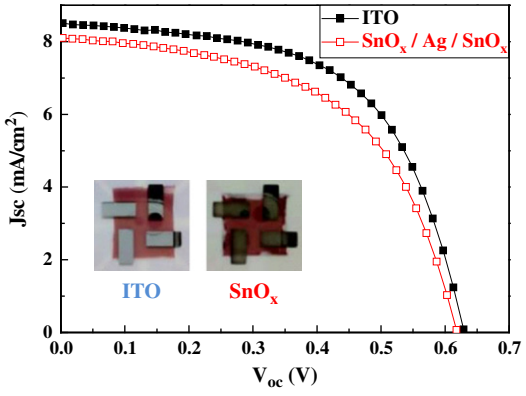

Fig. 8. Current density–voltage (J–V) characteristics under illumination of simulated AM 1.5 G (100 mW/cm^2) for the OPV fabricated on the SnO_x/Ag/SnO_x multilayer and on a commercial ITO.

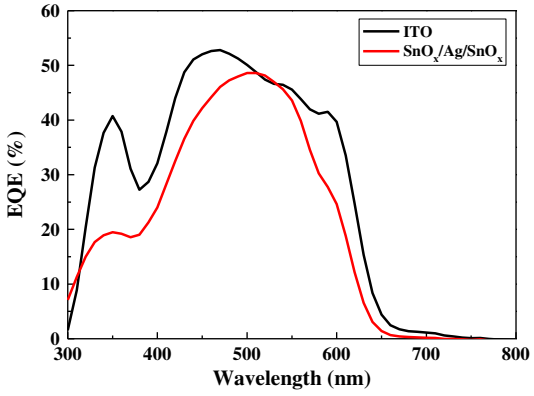

Fig. 9. External quantum efficiencies of OPV fabricated on ITO (black line) and SnO_x/Ag/SnO_x multilayer (red line).

600 nm through the optimized optical design. But series resistance should be also improved in the interface between the transparent electrode and the carrier transport layer to prevent J_{SC} from being decreased.

4. Conclusion

Indium-free $SnO_x/Ag/SnO_x$ multilayer transparent conducting electrodes with sheet resistance as low as 7.1 Ω/square and transmittance as high as 87.3% at 550 nm were deposited onto glass substrates, where their compatibility levels were evaluated as a reliable anode for normal OPVs. The resultant power conversion efficiency of 2.7% of the multilayer-based OPV device is slightly lower than that of the 3.09% of the reference ITO-based OPVs but is higher than any other OPV device on a multilayer TCO previously reported. This reveals that the $SnO_x/Ag/SnO_x$ multilayer is a promising transparent conducting electrode material for OPVs due to its very low resistivity, high transmittance, low temperature process, and low-cost components.

Acknowledgment

This research was supported by the Converging Research Center Program through the Ministry of Education, Science and Technology (2011K000592). This work was also partially supported by the KIST Foundation Research Program (2E22735).

References

[1] J.P. Kim, S.A. Lee, J.S. Bae, S.K. Park, U.C. Choi, C.R. Cho, Thin Solid Films 516 (2008) 5223.
[2] B.D. Ahn, Y.G. Ko, S.H. Oh, Thin Solid Films 517 (2009) 6414.
[3] S.H. Jeong, B.N. Park, S.B. Lee, J.H. Boo, Surf. Coat. Technol. 201 (2007) 5318.
[4] H.J. Cho, K.W. Park, J.K. Ahn, N.J. Seong, S.G. Yoon, W.H. Park, S.M. Yoon, D.J. Park, J.Y. Lee, J. Electrochem. Soc. 156 (8) (2009) J215.
[5] H. Han, N.D. Theodore, T.L. Alford, J. Appl. Phys. 103 (2008) 013708.
[6] A. Indluru, T.L. Alford, J. Appl. Phys. 105 (2009) 123528.
[7] S. Sutthana, N. Hongsith, S. Choopun, Curr. Appl. Phys. 10 (2010) 813.
[8] Y.Y. Choi, K.H. Choi, H.S. Lee, J.W. Kang, H.K. Kim, Sol. Energy Mater. Sol. Cells 95 (2011) 1615.
[9] Q. Kuang, C. Lao, Z.L. Wang, Z. Xie, L.Z., J. Am. Chem. Soc. 129 (2007) 6070.
[10] C. Waldauf, M. Morana, P. Denk, P. Schilinsky, K. Coakley, S.A. Choulis, C.J. Brabec, Appl. Phys. Lett. 89 (2006) 233517.
[11] E.D. Palik, Handbook of Optical Constants of Solids, Academic Press, Boston, 1985.
[12] G. Li, V. Shrotriya, J. Huang, Y. Yao, T. Moriarty, K. Emery, Y. Yang, Nat. Mater. 4 (2005) 864.
[13] S. Cook, R. Katoh, A. Furube, J. Phys. Chem. C 113 (2009) 2547.
[14] H.K. Yadav, K. Sreenivas, V. Gupta, Appl. Phys. Lett. 90 (2007) 172113.
[15] H. Han, N.D. Teodore, T.L. Alford, J. Appl. Phys. 103 (2008) 013708.
[16] G. Haacke, J. Appl. Phys. 47 (1976) 4086.
[17] J.C. Wang, W.T. Weng, M.Y. Tsai, M.K. Lee, S.F. Horng, T.P. Perng, C.C. Kei, C.C. Yu, H.F. Meng, J. Mater. Chem. 20 (2010) 862.
[18] J. Liu, A.W. Hains, J.D. Servaites, M.A. Ratner, T.J. Marks, Chem. Mater. 21 (21) (2009) 5258.
[19] Z. Hu, J.J. Zhang, Z.H. Hao, Q.Y. Hao, X.H. Geng, Y. Zhao, Appl. Phys. Lett. 98 (2011) 123302.
[20] H.K. Park, J.W. Kang, S.I. Na, D.Y. Kim, H.K. Kim, Sol. Energy Mater. Sol. Cells 93 (2009) 1994.